Optimal positioning of robot arms inside the abdominal cavity, to achieve optimal sight and range of motion in pediatric surgery

Research report clinical internship III

University of Twente
Technical Medicine
Medical Imaging & Interventions

Meander Medical Centre
Department of Surgery

University Medical Centre Groningen
Department of Surgery

Author
C.W.A. Pruijssers, BSc

Supervisors

Dr. J.L.M. Bruggink	Medical, UMCG
Dr. E.C.J. Consten	Medical, MMC/UMCG
Drs. R.H.J. de Kleine	Medical, UMCG
Prof. dr. S. Misra	Technical, University of Twente
Dr. J. Sikorski	Technical, University of Twente
N.S. Cramer Bornemann, MSc	Process, University of Twente

May 8, 2021

1 Introduction

Robot-assisted minimally invasive surgery (RMIS) in has shown increase in popularity in pediatric surgery due to improvements in visibility, accuracy and dexterity over conventional abdominal laparoscopy [1]. Articulated surgical tools, tremor filtering and 3D vision in RMIS can contribute to shorter hospital stay, lower conversion rates and fewer blood loss than in conventional laparascopic surgery [2–4].

Due to these advantages, RMIS appears to be usable for a number of abdominal pediatric surgical procedures. [1, 5]. In RMIS, the da Vinci™ XI Surgical System (Intuitive Surgical, Sunnyvale, USA) is one of the most advanced and widely used systems today. However, smaller pediatric abdominal volumes pose significant challenges for RMIS due to the size of the da Vinci XI system. In the smallest abdominal volumes it can impede the use of all four robotic arms impairing the surgeon to perform complex surgeries.

Robot mobility and patient safety of RMIS in smaller abdominal volumes is greatly dependent on the placement of the entry ports for the robotic arms [6]. Suboptimal port placement can cause compression injury and collision of the robotic arms, decreasing patient safety and surgery efficiency [1, 6]. Furthermore, universal placement guidelines are challenging to create in pediatric surgery due to widely varying abdominal sizes in pediatric patients warranting a more patient specific approach.

Optimization of port placement for pediatric RMIS based on pre-operative scans could help create patient specific insight on the effects of by port placement, such as collision chance, instrument reach and patient safety. In addition, it could aid the surgeon in deciding if using all four arms is a safe and efficient possibility for varying abdominal sizes.

However, optimizations aided by pre-operative imaging do not automatically take into account the insufflation of the abdomen needed in RMIS. Combining optimized port placement with a patient model of the insufflated abdomen should aid in a more patient specific and safe approach to pediatric RMIS.

Previous research by De Graaf and Rademakers [7, 8] has introduced a patient model consisting of the segmented abdomen, target organ and an estimation of the insufflated abdomen. The amount of abdominal distention due to insufflation was estimated with the abdominal dimensions. In further research by De Bock [9], a kinematic model of the Da Vinci Xi robot was made to describe different poses of the robot. In addition, an algorithm was written to optimize port placement on a simplified abdomen where port placements were categorized as 'safe' and 'unsafe'.

Although promising, both the patient model, kinematic model and optimization are still in the proof-of-concept phase and were separately developed. Further research is needed to join separate parts together in order to provide a better indication of the clinical impact of port optimization based on pre-operative scans. Visualization of changes in robot mobility and patient safety caused by port placement in robot should create insight in the possibilities of RMIS in pediatric surgery. In addition, This research aims to improve upon the current kinematic model & optimization and link it with the existing patient model to guide the pediatric surgeon in more optimized port placement.

2 Methods

2.1 Study design

Expansions are made on contributions of previous research is and separate parts are joined together for a complete workflow. An overview of the proposed workflow and its parts is shown in figure 1. Intra-operative measurements of the insufflated abdomen were taken with a depth camera to quantify abdominal distention. The previous kinematic model was updated with visualizations and more accurate collision geometry. Previous port optimization was simplified and robot movement was simulated for better assessment of robot performance.

2.2 Patient model

Previous research by De Graaf en Rademaker estimated the amount of abdomen distention due to intra-operative insufflation with the help of the dimensions of the abdomen segmentation. An ellipsoid was created with estimated radius in x,y and z directions based on craniocaudal, lateral and ventrodorsal lengths of the abdomen respectively. In order to validate these estimations of abdomen distention a measurement protocol was created for 3D scanning of the intra-operative insufflation.

The infrared camera of a Kinect V1 sensor (Microsoft, Redmond, USA) was used to measure depth points on the abdomen of a 23 month old patient before and after insufflation. The Kinect for Windows Software Developer Kit (SDK) is open source software that enables the extraction of the depth information acquired by the sensor. Kinect Fusion is an

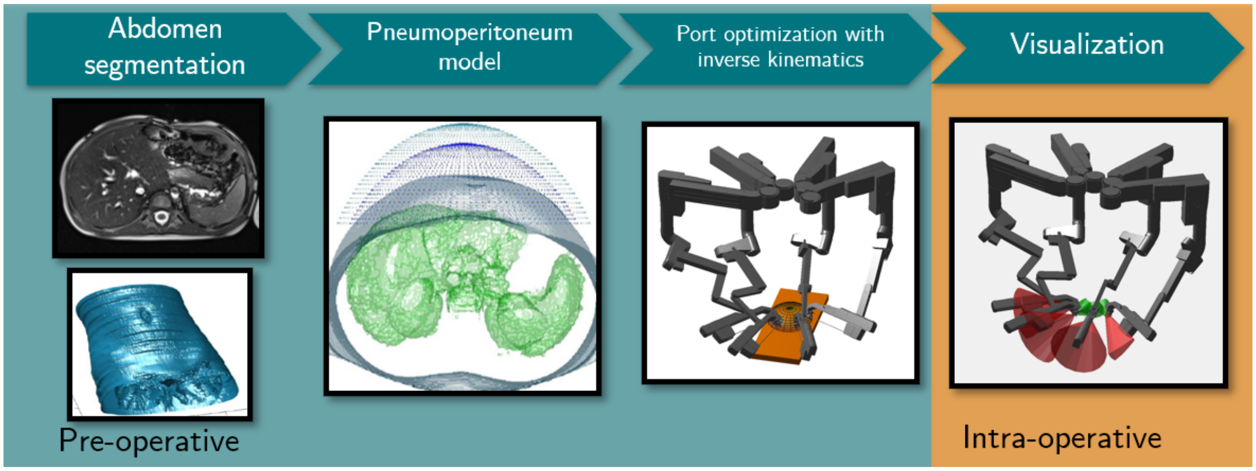

Figure 1: Depiction of the proposed method for port optimalisation

app in the SDK that enables the conversion of depth information averaged over multiple frames into a 3D scan of the object. A scan of the abdomen can be taken quickly (10 to 20 seconds) by moving the sensor around the abdomen in lateral direction standing from the caudal side of the patient, see figure 2. This enables easy use without infringing the sterile environment with minimal time loss.

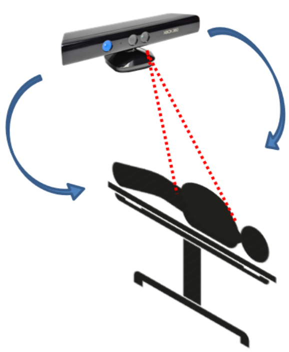

Figure 2: Visualisation of measurement protocol of 3D scanning of the insufflated abdomen with the Kinect Sensor

Settings of the Kinect Fusion app were tested on a healthy subject before intra-operative use . Settings were optimized for the largest resolution scan possible with a distance of 0.5 to 3 meters with a Lenovo Thinkpad P1 (Intel Core i7-10750H, NVIDIA Quadro T2000). Finalized settings for the Kinect Fusion app are shown in table 1

Afterwards, the resulting 3D point clouds were cropped and rotated. Detailed cropping was done in the open source software Meshlab (ISTI-CNR, Pisa, Italy). Key points for registration were selected

Table 1: Settings for the Kinect Fusion app

Depth Threshold min/max (m)	0.35 - 3.00
Volume max integration weight	400
Volume voxels per meter	384
Volume voxels resolution (x,y,z)	640

in MATLAB (Mathworks, Natick, USA), at rigid points that are unaffected by insufflation. Points were located bilaterally at spina iliaca anterior superior (SIAS) and at the costal arch at the same lateral location of the SIAS [10], see figure 3. Registered point clouds were converted to 3D surfaces with delaunay triangulation as implemented in MATLAB by Giaccari [11].

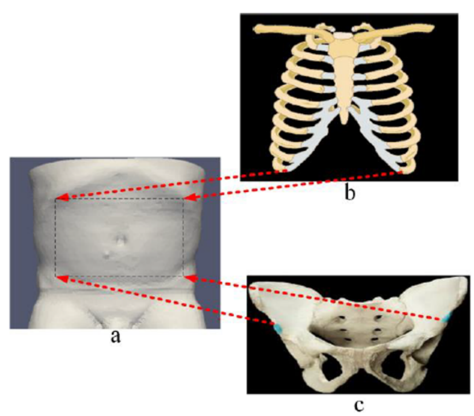

Figure 3: Rigid points used for the registration of pre- and post-insufflation surfaces [10]

To quantify abdomen distention, the difference between the highest point after insufflation and its corresponding point before insufflation was measured in ventrodorsal direction. The radius of the insufflated abdomen in lateral en craniocaudal directions were estimated from this highest point.

2.3 Kinematic model

The kinematic model available from earlier research by De Bock was updated with a CAD model of the da Vinci XI system [12]. Separate .stl files of 3D models of the robot links were extracted in 3dsMax (Autodesk, San Rafael, USA). In MATLAB, the 3D models of the links were coupled to their respective joints. In order to synchronize the pose and dimensions of the link models with the kinematic model, the files were scaled, rotated and translated to align them with their respective coordinate system. Scaling factors were determined with measured dimensions of the da Vinci XI system.

Previously available collision geometry was adjusted to the new visualisation of the kinematic model. In addition, collision geometry was added for the surgery table and the patient for a more complete collision environment.

The frames of the joints of the da Vinci XI are described with Denavit Hartenberg (DH) parameters as stated by Ferguson et al. [13]. The final three joints were fixed in order to simplify the kinematic model and subsequent simulations, see figure 4.

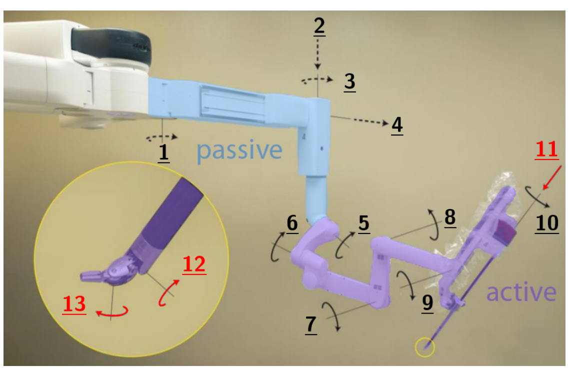

Figure 4: Kinematic chain of one of the da Vinci Robotic arms. Passive sections are blue and active sections are in blue. Red arrows indicate joints that are fixed for simplification of the kinematic model

2.4 Port optimalisation

2.4.1 Docking

In RMIS, the da Vinci XI system is docked to the patient by connecting the arms of the robot to the entry points and aiming them at the target organ. After docking, the first four passive joints are no longer used in movement of the robotic arm.

The docking procedure was simulated by creating a generalized inverse kinematics (GIK) solver with the robotics toolkit available in MATLAB. The GIK solver calculates poses for the robot arms taking into account constraints on the solution. For the docking procedure the end of the tool was constrained to the port location for each arm. In addition, an aiming constraint for the tool was applied so each tool was aiming at the target organ. The resulting poses of the arms were checked for collision. If an arm collided with another arm, the patient or the table, the joint positions of link 5 and 6 (see figure 4 were randomized until no collision was detected. These joints were chosen for randomisation because they move the arms towards or away from each. Other joint positions were left unchanged to preserve the general position of the robot.

2.4.2 Motion simulation

After docking, the first four joints were locked in their respective positions for the next step. Each arm of the da Vinci XI system has a remote centre of motion (RCM) located at the port. The position of the RCM remains unchanged which prevents the displacement of the port location. Subsequently, the tool was inserted into the patient at the port to depth r. Coordinates of a spherical trajectory for are defined with the following equations for $0 < \theta < \pi$ and $0 < \phi < 2\pi$:

$$x = r * sin(\theta) * cos(\phi) \tag{1}$$
$$y = r * sin(\theta) * sin(\phi) \tag{2}$$
$$z = r * cos(\theta) \tag{3}$$

Depth r serves as a radius from the RCM to the tip of the instrument at the end of the robotic arm. The created spherical trajectory describes the movement possible for an arm inserted at depth r , see figure 5. The trajectory was cropped to fit approximately inside the patient model to exclude unrealistic movement.

A second GIK solver was created with constraints to keep the port in place and follow the created trajectory with the tip of the tool. Collision with the table and patient was checked at each point of the trajectory.

Afterwards, the occupied volume during the movement of the last external link and the internal part of the instrument is visualized. The last external link was chosen for visualisation because it is one of the most common links for collision.

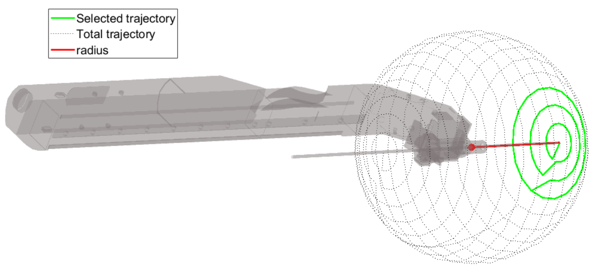

Figure 5: End-effector tool of the da Vinci XI arm with planned trajectory simulating the possible movement with the port as rotation centre. The red dot in the image is the port location

3 Results

3.1 Patient model

Resulting surfaces of the abdomen depth measurements pre- and post-insufflation are depicted in figure 6. The highest point of insufflation was found approximately 2 cm cranially of the umbilicus. At this point, distention in the ventrodorsal direction was 3.6 cm. Radii of the insufflated abdomen relative to the highest point were 9.4 and 10.2 cm in the lateral and craniocaudal directions respectively. Measurements were taken at a pressure of 8 mmHg of CO_2.

3.2 Kinematics

A docking configuration was solved with the previously described GIK solver and constraints for example set for port placement. The kinematic model with visualized links is shown in the calculated docking configuration along with patient en surgery table geometries in figure 7. Over five tries, docking took an average of 45±15 seconds.

Resulting trajectory of the leftmost arm inside the patient with the instrument inserted half its maximum length is shown in figure 10. For each point the deviation from the planned trajectory is calculated to assess precision of The visualisation of the occupied volume of the robotic arms during the trajectory movement is seen in figure 9. Over five docking configurations, trajectory calculation with a tolerance of 1 mm took approximately 789±64 seconds for 60 trajectory points.

4 Discussion

The presented measurement protocol for abdomen distention showed a proof-of-concept for a quick method to quantify abdomen insufflation. Measurements of abdomen distention enable validation of current estimations of the insufflated abdomen which should benefit the accuracy and patient specificity for the complete workflow.

Improved kinematics of the previous research enabled optimisation of the robot based around movement of the robotic arm instead of static poses. Dynamic optimization should provide a better assessment of robot mobility at different port placements. Improved optimization combined with a more accurate visual representation of the robot should provide more insight in the consequences of port placement in robot mobility and patient safety without a trial-and-error approach on patients.

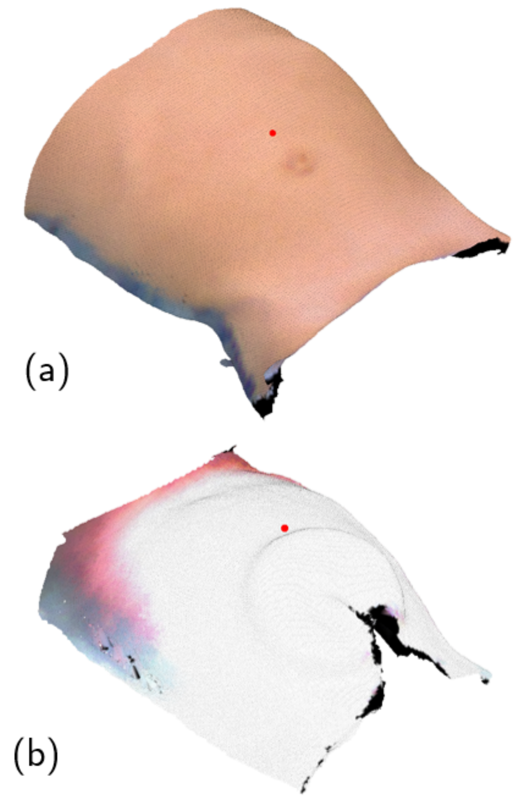

Figure 6: Surfaces of abdomen of 23 month old subject **(a)** Pre-insufflation **(b)** Post-insufflation. Red dots indicate the point of maximum distention in ventrodorsal direction

4.1 Patient model

Depth measurements showed a viable method to quantify abdomen distention. However, validation of previous estimations of abdomen insufflation was not feasible for the measured subject be-

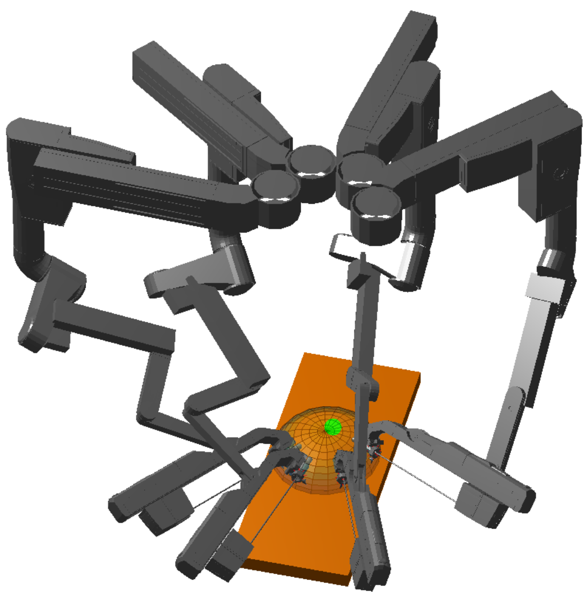

Figure 7: Resulting docking configuration returned by the GIK solver with table and patient geometry. The green dot indicates the target

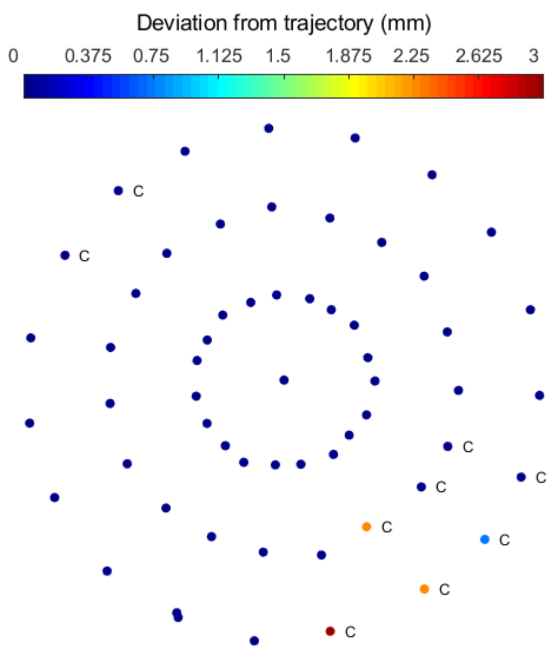

Figure 8: 2D view of the realised trajectory. The color indicates how much the position of the tool deviates from the planned trajectory in millimeters. Point labeled with a 'c' are point where the arm collided with the table.

cause the pre-operative scans were not available. In further research, comparing estimated abdomen

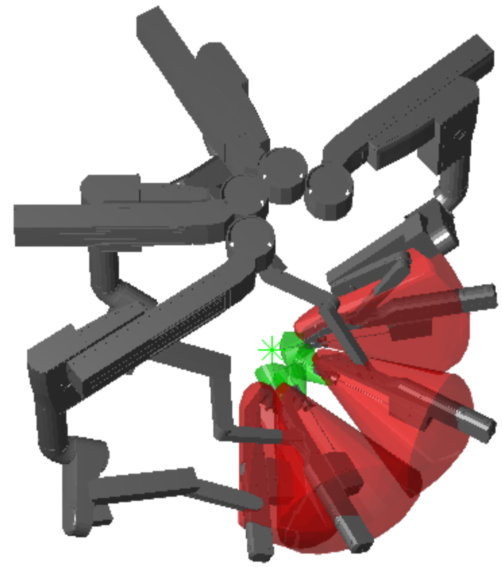

Figure 9: Occupied volumes during trajectory of the last external link (red) and the internal part of the tool (green)

distention with measured intra-operative distention should be able to provide insight about the accuracy of the current approach.

Registration of both point clouds was done on points unaffected by abdomen distention. However, due to bright surgical lights the color was lost on the post insufflation depth measurements. Consequently, anatomical landmarks used for registration were harder to pinpoint due to the loss of texture. In addition, the laparoscopic Alexis port obstructs clear view of the abdomen which impairs accurate selection of the highest point on the abdomen.

During surgery, and in the 3D surfaces it can be observed that the abdomen distention is not a perfect ellipsoid. This is most likely caused by varying mechanical tissue properties and distribution of skeletal connections of the abdominal wall. Other research has shown the use of FEM analysis to simulate the irregular distention of the abdomen [14–16]. The current segmentation approach results in surface meshes which are insufficient for FEM analysis. Using readily available software such as the Iso2Mesh toolbox [17] can convert surface meshes to tetrahedral volume meshes suitable for FEM analysis. Further research in FEM analysis could yield a better simulation of the irregular distention of the abdomen during intra-operative insufflation.

4.2 Kinematics

GIK solvers for docking and trajectory movement showed promising results for simulating the movement at different port locations. Although the MATLAB robotics toolbox is easy to use, it is a 'black box' where intermediate steps of the solver can not be evaluated by the user. The inability to easily understand and debug unrealistic results returned by the solver reduces the flexibility of the approach to create a tailor made solution for the port optimization problem. Further research could benefit from creating their own solver in order to gain more control over the optimization results.

4.2.1 Visualisation

The acquired 3D CAD model from Dabronaki [12] was adjusted to fit the kinematic model as described by Ferguson et al [13]. However, while the 3D model looked visually correct the dimensions and ratios of the model did not coincide with the kinematic model. Each link of the robot was scaled and edited separately to fit the model as best as possible. A simplified separate .stl file for link 6 of the robotic arm was created due to large inaccuracies in the 3D model. Although the visualization provides a intuitive and familiar view for the robot for easy interpretation, it should not be used for collision or joint limit assessment. For this reason and added time constraints, the collision geometry was made from simplified cylinders and boxes based on physical measurements of the robot.

4.2.2 Docking

In its current state, a docking configuration is reached with randomized positions of joints 5 and 6 resulting in different poses and subsequent performance when following the trajectories.

In order to counteract randomness, a measure is needed to estimate performance of the robot arm at a certain port location. Performance was attempted to be estimated with the manipulability index as introduced by Yoshikawa [18]. The index is defined as $\sqrt{det(J * J^T)}$ where J is the geometric Jacobian. However, this measure does not take into account the constraint of the port position. An augmented Jacobian could provide more and faster insight in the performance at a certain docking position while taking into account the port constraint for better optimisation [19,20].

In addition, random docking sometimes resulted in links 7 and 8 being fully stretched due to unrealistic positioning of the first four joints, see the rightmost arm in figure 7. The robot arm was subsequently severely impaired during movement after locking the first four arms, **??**. Docking needs to be further optimised with a index like the manipulability index or other constraints to prevent unrealistic docking configurations.

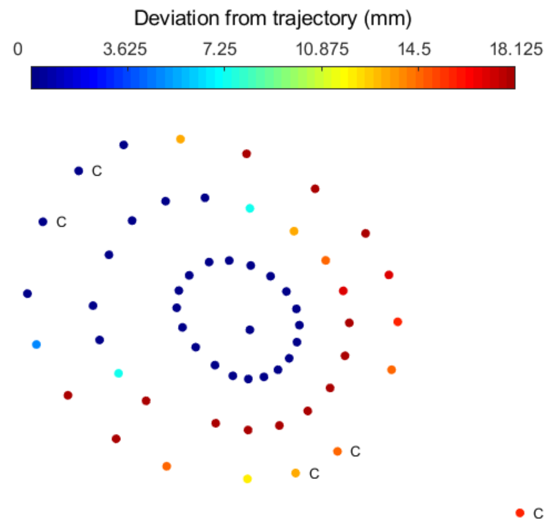

Figure 10: 2D view of realised trajectory of. The color indicates how much the position of the tool deviates from the planned trajectory in millimeters. Point labeled with a 'c' are point where the arm collided with the table.

4.2.3 Motion simulation

In its current state, the optimisation allows movement of the robotic arms for insight of the consequences of port placements. Initially, the aim of the research was to calculate indices for collision chance [21] and instrument cooperation [22]. These goals were not met due to time constraints. However, required volumes for the indices are available and could easily be incorporated in further research. This should enable quantification of robot performance at different port placements for easy comparison of different port configurations.

Animations of the found robotic arms following the spherical trajectories could sometimes show large pose differences between consecutive trajectory points. This was caused by a joint wrapping around their joint limits to reach the target point.

4.3 Future research

Combining parts of earlier research has resulted in a complete pipeline for port optimization. Although more research is needed for the patient and kinematic model, the ultimate goals is to transfer this proof-of-concept pipeline to a phantom study before clinical implementation. To assess clinical viability the most important step is to finish quantification of robot performance for easy interpretation for the surgical team. With this, a complete proof-of-concept can be tested and validated in a phantom study.

A suitable phantom study could consist of different sized ellipsoidal abdomens simulating the varying abdomen size in pediatric surgery. Comparison between port placement as indicated by the surgical experts and port optimization algorithm could assess if the optimization adds to the performance of the robot. Certain motions i.e. suturing could be tested with both port configurations to test the kinematic modelling of the robot which should assess the viability of clinical implementation of the proposed method.

5 Conclusion

In this research a more complete pipeline for port optimization for pediatric RMIS is presented through improvements and combinations of earlier research. A initial proof-of-concept for port optimization on a simplified ellipsoidal abdomen with simulated movement of the robotic arm. Further research is needed to further quantify performance of the robotic arms at different port placement for more insight. In addition, to assess the viability of clinical implementation it is essential to aim for a phantom study to validate the simulated robot performance. A phantom study should provide insight about the expected performance in its current state and indicate the amount of additional research needed for a model accurate enough to safely aid in port placement in surgical RMIS.

References

[1] Girolamo Mattioli and Paolo Petralia. *Pediatric Robotic Surgery*. 2017.

[2] Ferdinand Köckerling. Robotic vs. Standard Laparoscopic Technique – What is Better? *Frontiers in Surgery*, 1(May):10–13, 2014.

[3] Hiroyuki Koga, Hiroshi Murakami, Takanori Ochi, Go Miyano, Geoffrey J. Lane, and Atsuyuki Yamataka. Comparison of robotic versus laparoscopic hepaticojejunostomy for choledochal cyst in children: a first report. *Pediatric Surgery International*, 35(12):1421–1425, 2019.

[4] Naved K. Alizai, Michael J. Dawrant, and Azad S. Najmaldin. Robot-assisted resection of choledochal cysts and hepaticojejunostomy in children. *Pediatric Surgery International*, 30(3):291–294, 2014.

[5] Aayed Alqahtani, Abdullrahman Albassam, Mohammed Zamakhshary, Mohammed Shoukri, Tariq Altokhais, Ayman Aljazairi, Abdullrhman Alzahim, Mohammed Mallik, and Abdullah Alshehri. Robot-assisted pediatric surgery: How far can we go? *World Journal of Surgery*, 34(5):975–978, 2010.

[6] Charles Chang, Zoe Steinberg, Anup Shah, and Mohan S. Gundeti. Patient positioning and port placement for robot-assisted surgery. *Journal of Endourology*, 28(6):631–638, 2014.

[7] Pien de Graaf. Optimal Positioning of Robotic Arms Inside the Abdominal Cavity in Pediatric Surgery. 2020.

[8] Fenna Rademaker. Optimal Positioning of Robotic Arms in Pediatric Robotic Surgery : a Trocar Placement Model. 2020.

[9] Eva Bock de. Optimisation of port placement in paediatric robot-assisted laparoscopic surgery using the da Vinci Xi. 2021.

[10] Mohammad Reza Maddah. 3D visualization and interactive image manipulation for surgical planning in robot-assisted surgery. 2019.

[11] Luca Giaccari. Surface Reconstruction from scattered points cloud (open surfaces), 2021.

[12] David Dabronaki. Surgical System da Vinci Xi 3D model, 2020.

[13] James M. Ferguson, Bryn Pitt, Alan Kuntz, Josephine Granna, Nicholas L. Kavoussi, Naren Nimmagadda, Eric J. Barth, Stanley Duke Herrell, and Robert J. Webster. Comparing the accuracy of the da Vinci Xi and da Vinci Si for image guidance and automation. *International Journal of Medical Robotics and Computer Assisted Surgery*, 16(6):1–10, 2020.

[14] J. Bano, A. Hostettler, S. A. Nicolau, S. Cotin, C. Doignon, H. S. Wu, M. H. Huang, L. Soler, and J. Marescaux. Simulation of pneumoperitoneum for laparoscopic surgery planning. *Lecture Notes in Computer Science (including subseries Lecture Notes in Artificial Intelligence and Lecture Notes in Bioinformatics)*, 7510 LNCS:91–98, 2012.

[15] Shivali Dawda, Mafalda Camara, Philip Pratt, Justin Vale, Ara Darzi, and Erik Mayer. Patient-Specific Simulation of Pneumoperitoneum for Laparoscopic Surgical Planning. *Journal of Medical Systems*, 43(10), 2019.

[16] Yukitaka Nimura, Jia Di Qu, Yuichiro Hayashi, Masahiro Oda, Takayuki Kitasaka, Makoto Hashizume, Kazunari Misawa, and Kensaku Mori. Pneumoperitoneum simulation based on mass-spring-damper models for laparoscopic surgical planning. *Journal of Medical Imaging*, 2(4):044004, 2015.

[17] Qianqian Fang and David A. Boas. Tetrahedral mesh generation from volumetric binary and grayscale images. In *2009 IEEE International Symposium on Biomedical Imaging: From Nano to Macro*, pages 1142–1145, 2009.

[18] Tsuneo Yoshikawa. Manipulability of Robotic Mechanisms. *International Journal of Robotics Research*, 4(2):3–9, 1985.

[19] Juan Sandoval, Gerard Poisson, and Pierre Vieyres. A new kinematic formulation of the RCM constraint for redundant torque-controlled robots. *IEEE International Conference on Intelligent Robots and Systems*, 2017-September(October):4576–4581, 2017.

[20] Adria Colome and Carme Torras. Redundant inverse kinematics: Experimental comparative review and two enhancements. *IEEE International Conference on Intelligent Robots and Systems*, pages 5333–5340, 2012.

[21] Robert G. Stricko, Brett Page, Amy E. Kerdok, Brandon Itkowitz, and Jason Pile. Port placement optimization for robotically-assisted minimally invasive surgery. *Frontiers in Biomedical Devices, BIOMED - 2018 Design of Medical Devices Conference, DMD 2018*, pages 1–4, 2018.

[22] Fan Zhang, Zhiyuan Yan, and Zhijiang Du. Preoperative planning for the multi-arm surgical robot using PSO-GP-based performance optimization. *Proceedings - IEEE International Conference on Robotics and Automation*, pages 4208–4214, 2017.